

N,S-Doped Porous Carbon Nanobelts Embedded with MoS₂ Nanosheets as a Self-Standing Host for Dendrite-Free Li Metal Anodes

Binke Li, Weishan Cao, Shuaize Wang, Zhenjiang Cao, Yongzheng Shi, Jin Niu,* and Feng Wang*

Metallic Li is one of the most promising anodes for high-energy secondary batteries. However, the enormous volume changes and severe dendrite formation during the Li plating/stripping process hinder the practical application of Li metal anodes (LMAs). We have developed a sulfate-assisted strategy to synthesize a self-standing host composed of N,S-doped porous carbon nanobelts embedded with MoS₂ nanosheets (MoS₂@NSPCB) for use in LMAs. In situ measurements and theoretical calculations reveal that the uniformly distributed MoS₂ derivatives within the carbon nanobelts serve as stable lithiophilic sites which effectively homogenize Li nucleation and suppress dendrite formation. In addition, the hierarchical porosity and 3D nanobelt networks ensure fast Li-ion diffusion and accommodate the volume change of Li deposits during the plating/stripping process. As a result, a Li–Li symmetric cell using the MoS₂@NSPCB host operates steadily over 1500 h with an ultralow voltage hysteresis (≈ 24.2 mV) at 3 mA cm⁻²/3 mAh cm⁻². When paired with a LiFePO₄ cathode, the current collector-free LMA endows the full cell with a high energy density of 460 Wh kg⁻¹ and good cycling performance (with a capacity retention of $\approx 70\%$ even after 1600 cycles at 10 C).

1. Introduction

The energy densities of Li-ion batteries based on graphite anodes cannot meet the ever-increasing energy demands of electric vehicles and power stations.^[1,2] Metallic Li is considered an ideal anode material for high-energy rechargeable batteries because of its ultrahigh theoretical specific capacity (3860 mAh g⁻¹) and ultralow electrochemical potential (-3.04 V vs standard hydrogen electrode).^[3] Unfortunately, the practical application of Li metal anodes (LMAs) involves two major challenges—undesirable dendrite formation and enormous volume change—which continuously decompose the electrolyte by destroying/rebuilding the solid electrolyte interface (SEI), and can even cause a short circuit leading to potential safety problems.^[4–7]


Many strategies have been proposed to improve LMAs, including designing liquid/solid electrolytes, constructing artificial SEIs, and introducing 3D hosts.^[8–11] Pre-storing Li in 3D hosts can efficiently

regulate the electric fields governing Li-ion transport resulting in uniform current distributions for Li nucleation and growth.^[12–15] Carbon-based frameworks are ideal hosts for high-performance LMAs because of their excellent electrical conductivity and high electrochemical stability.^[16] However, the lithiophobic nature of carbon materials results in high barriers for Li nucleation, resulting in an inability to regulate subsequent Li growth.^[17] Although a variety of metal and non-metal atoms and their compounds have been introduced into a carbon matrix in an attempt to change the surface chemistry of the carbon-based hosts,^[18–20] some issues remain unresolved: i) complicated preparation procedures are usually required to ensure the efficient introduction of lithiophilic sites; ii) how to balance the conflicting requirements of high structural stability and high surface activity of lithiophilic sites; iii) hosts having both abundant lithiophilic sites and good mechanical properties are difficult to fabricate; iv) mechanisms of host modification in LMAs are not well understood.

We report the use of a simple sulfate-assisted method to fabricate a new self-standing host consisting of N,S-doped carbon nanobelts with hierarchical porosity impregnated with MoS₂

B. Li, W. Cao, S. Wang, Z. Cao, Y. Shi, J. Niu, F. Wang
State Key Laboratory of Chemical Resource Engineering
Laboratory of Electrochemical Process and Technology for Materials
Beijing University of Chemical Technology
Beijing 100029, P. R. China
E-mail: niujin@mail.buct.edu.cn; wangf@mail.buct.edu.cn

B. Li, W. Cao, S. Wang, Y. Shi, J. Niu, F. Wang
Beijing Advanced Innovation Center for Soft Matter Science and
Engineering
Beijing University of Chemical Technology
Beijing 100029, P. R. China

 The ORCID identification number(s) for the author(s) of this article can be found under <https://doi.org/10.1002/advs.202204232>

© 2022 The Authors. Advanced Science published by Wiley-VCH GmbH. This is an open access article under the terms of the Creative Commons Attribution License, which permits use, distribution and reproduction in any medium, provided the original work is properly cited.

DOI: 10.1002/advs.202204232

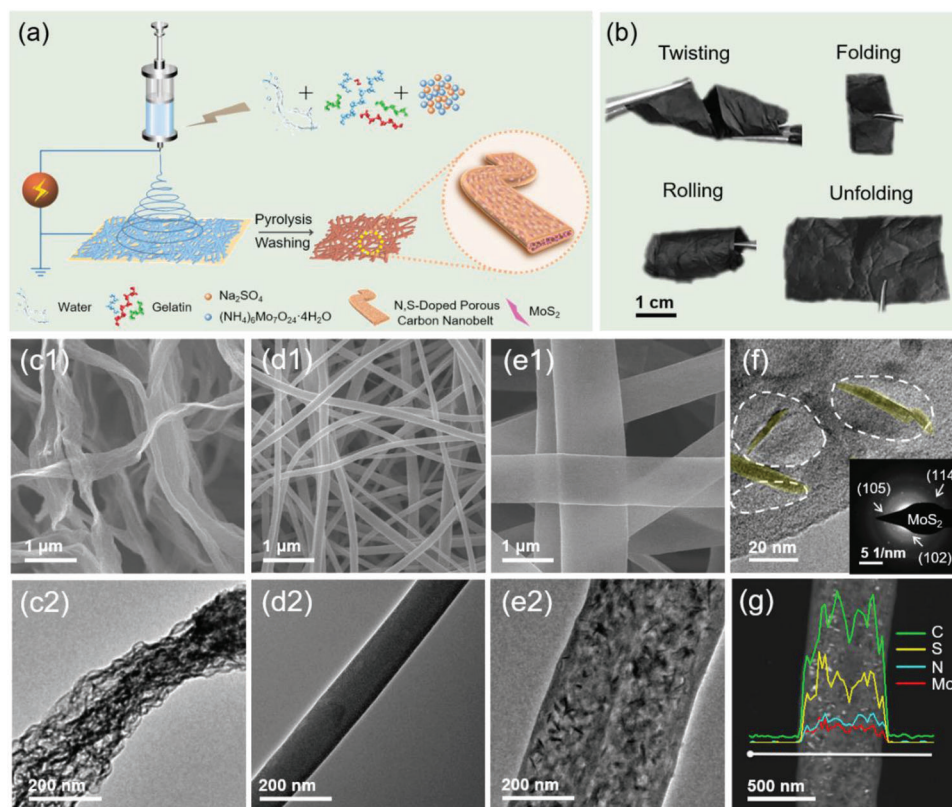


Figure 1. a) Schematic illustration of the synthesis of MoS_2 @NSPCB films. b) Digital photos showing the flexibility of the MoS_2 @NSPCB film in various states, including twisting, rolling, and folding. SEM images of (c1) NSPCB, (d1) MoO_x @NCF, and (e1) MoS_2 @NSPCB. TEM images of (c2) NSPCB, (d2) MoO_x @NCF, and (e2) MoS_2 @NSPCB. f) High-resolution TEM image (inset: selected area electron diffraction pattern) and g) EDX linear scanning analysis of MoS_2 @NSPCB.

nanosheets (denoted as MoS_2 @NSPCB). The MoS_2 @NSPCB host has abundant metal/non-metal lithiophilic sites facilitating uniform Li nucleation. Additionally, the hierarchical porosity and N,S-doped carbon support endow the lithiophilic sites with good structural stability as well as high surface chemical activity. Moreover, the 3D conductive nanobelt networks ensure fast Li-ion diffusion, preventing the formation of dendrites in the LMA during the plating/stripping process. LMAs based on the MoS_2 @NSPCB host show excellent performance in half cells. Furthermore, the current collector-free LMAs endow full cells with high energy density, long cycling and fast-charge/discharge performance.

2. Results and Discussion

Figure 1a shows a schematic illustration of the synthesis for the MoS_2 @NSPCB host. An aqueous solution of gelatin containing Na_2SO_4 and ammonium molybdate ($(\text{NH}_4)_6\text{Mo}_7\text{O}_{24}\cdot 4\text{H}_2\text{O}$) was used to electrospin films, which were then pyrolyzed and washed with deionized water. In contrast to previously reported gelatin-derived carbon films, the MoS_2 @NSPCB film shows superb flexibility as a self-standing host (Figure 1b). Two other gelatin-derived carbon samples were prepared using the same procedure, one without Na_2SO_4 and the other without ammonium molybdate. As shown in Figure S1 (Supporting Information), the former (denoted as MoO_x @NCF) is also a self-standing film,

while the latter (denoted as NSPCB) is easily broken into small pieces, indicating that the introduction of ammonium molybdate improves the mechanical strength of the final samples due to the coordination between Mo centers and functional groups in gelatin.^[21,22]

X-ray diffraction (XRD) and Raman spectroscopy confirm the presence of gelatin-derived carbons in all three samples (Figure S2, Supporting Information). Characteristic peaks of MoS_2 are observed in the XRD pattern and Raman spectrum of MoS_2 @NSPCB, while no characteristic peaks of Mo compounds are shown in those of MoO_x @NCF. Due to the similar weight content of noncarbon materials for MoO_x @NCF and MoS_2 @NSPCB ($\approx 40\%$, Figure S3, Supporting Information), the metallic compound within MoO_x @NCF is considered to have an amorphous structure. X-ray photoelectron spectroscopy (XPS, Figure S4, Supporting Information) confirms that MoO_x and MoS_2 are present in MoO_x @NCF and MoS_2 @NSPCB, respectively.^[23] This suggests that Na_2SO_4 acts as a sulfurizing reagent and reacts with molybdate ions to form MoS_2 . N species are observed in the XPS spectra of all the samples and additional S species are observed in the XPS spectra of NSPCB and MoS_2 @NSPCB, suggesting that Na_2SO_4 also plays a role as a dopant by introducing S heteroatoms into the carbon framework.

The addition of Na_2SO_4 not only affects the chemical composition but also regulates the structural morphology of the samples.

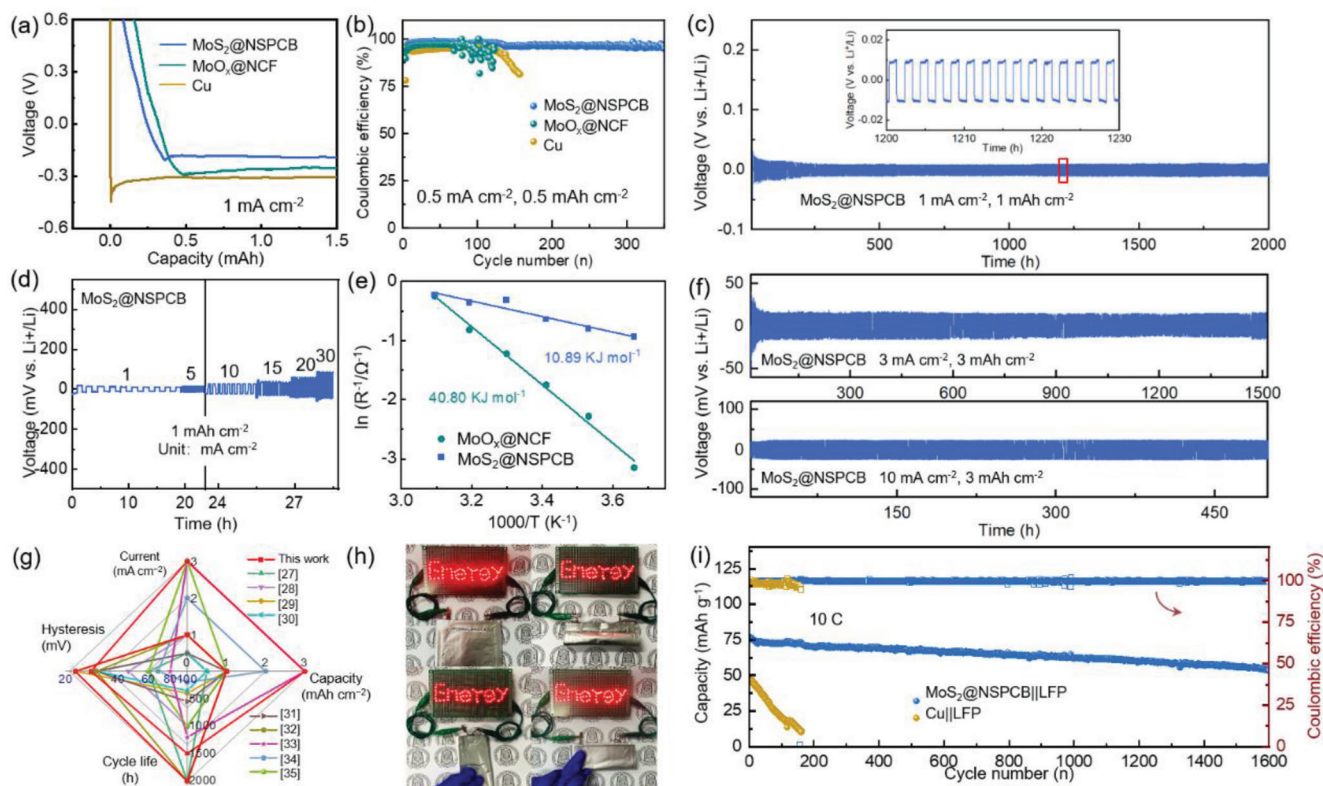


Figure 2. a) The voltage–capacity curves in the initial cycle and b) Coulombic efficiency (the initial cycle is not shown) of Li|Cu, Li|MoO_x@NCF, and Li|MoS₂@NSPCB half cells. c,d) Galvanostatic cycling performance of Li|Li symmetric cells using MoS₂@NSPCB hosts at different current densities. e) Activation energy for Li-ion diffusion with the MoS₂@NSPCB and MoO_x@NCF hosts. f) Galvanostatic cycling performance of Li|Li symmetric cells using MoS₂@NSPCB hosts with plating/stripping capacity of 3 mAh cm⁻². g) Comparison of the electrochemical performance of Li|Li symmetric cells using the MoS₂@NSPCB host with the cells using other hosts. h) Digital photos of a MoS₂@NSPCB-Li|LiFePO₄ pouch cell powering LED lights in different states. i) Cycling performance of the MoS₂@NSPCB-Li|LiFePO₄ and Cu-Li|LiFePO₄ full cells.

Scanning electron microscopy (SEM) results (Figure 1c1–e1) show that NSPCB and MoS₂@NSPCB have ultrathin nanobelt structures, while MoO_x@NCF has a nanofiber structure. This suggests that Na₂SO₄ can influence the rheological or other properties of the solution and favor the formation of a nanobelt structure during the electrospinning process (Figure S5, Supporting Information). Transmission electron microscopy (TEM) images show that obvious pores exist in NSPCB and MoS₂@NSPCB, while no pores can be observed in MoO_x@NCF (Figure 1c2–e2). N₂ adsorption/desorption measurements verify the hierarchical porosities of NSPCB and MoS₂@NSPCB and the non-porous structure of MoO_x@NCF, suggesting that Na₂SO₄ also acts as a template for nanopore formation (Figure S6, Supporting Information). Well-dispersed nanosheets are observed in MoS₂@NSPCB (Figure 1f; and Figure S7, Supporting Information), which are confirmed to be MoS₂ by selected area electron diffraction (Figure 1f, inset).^[24,25] It should be noted that these MoS₂ nanosheets are embedded within the porous carbon nanobelts since they are unobservable in the SEM image. Energy dispersive X-ray (EDX) results of MoS₂@NSPCB are displayed in Figure 1g; and Figure S7d (Supporting Information). The linear scanning curves exhibit a mesa-like shape, characteristic of a nanobelt structure. The high dispersion of C, N, and S in the

elemental mapping images indicate that N/S atoms are doped in the carbon nanobelts, consistent with the XPS results.

The self-standing films of MoS₂@NSPCB and MoO_x@NCF were used as hosts for LMAs. Li|Cu, Li|MoO_x@NCF, and Li|MoS₂@NSPCB half-cells were assembled in order to compare the Li plating/stripping behaviors. As shown in **Figure 2a**, the MoS₂@NSPCB host displays the smallest overpotential for Li nucleation and plating in the initial cycle, corresponding to the lowest nucleation barrier and fastest Li-ion migration.^[15] Moreover, the Li|MoS₂@NSPCB cell performs the highest Coulombic efficiency of all the cells with a good cycling performance over 350 cycles at 0.5 mA cm⁻² for 0.5 mAh cm⁻² (Figure 2b). An average Coulombic efficiency of ≈99% was obtained at 1 mA cm⁻² for 1 mAh cm⁻² (Figure S8, Supporting Information), indicative of the high reversibility of Li plating/stripping in the MoS₂@NSPCB host. Symmetric cells were assembled to evaluate the galvanostatic cyclic performance and the interfacial stability of the LMAs with and without the hosts. At a current of 1 mA cm⁻² for 1 mAh cm⁻², a Li|Li symmetric cell using the MoS₂@NSPCB host shows a stable cycling life over 2000 h with an ultralow voltage hysteresis of ≈22.7 mV (Figure 2c). In contrast, Li|Li symmetric cells with the MoO_x@NCF host and Cu foil display high voltage hysteresis of ≈73.0 and ≈53.0 mV, respectively (Figure S9,

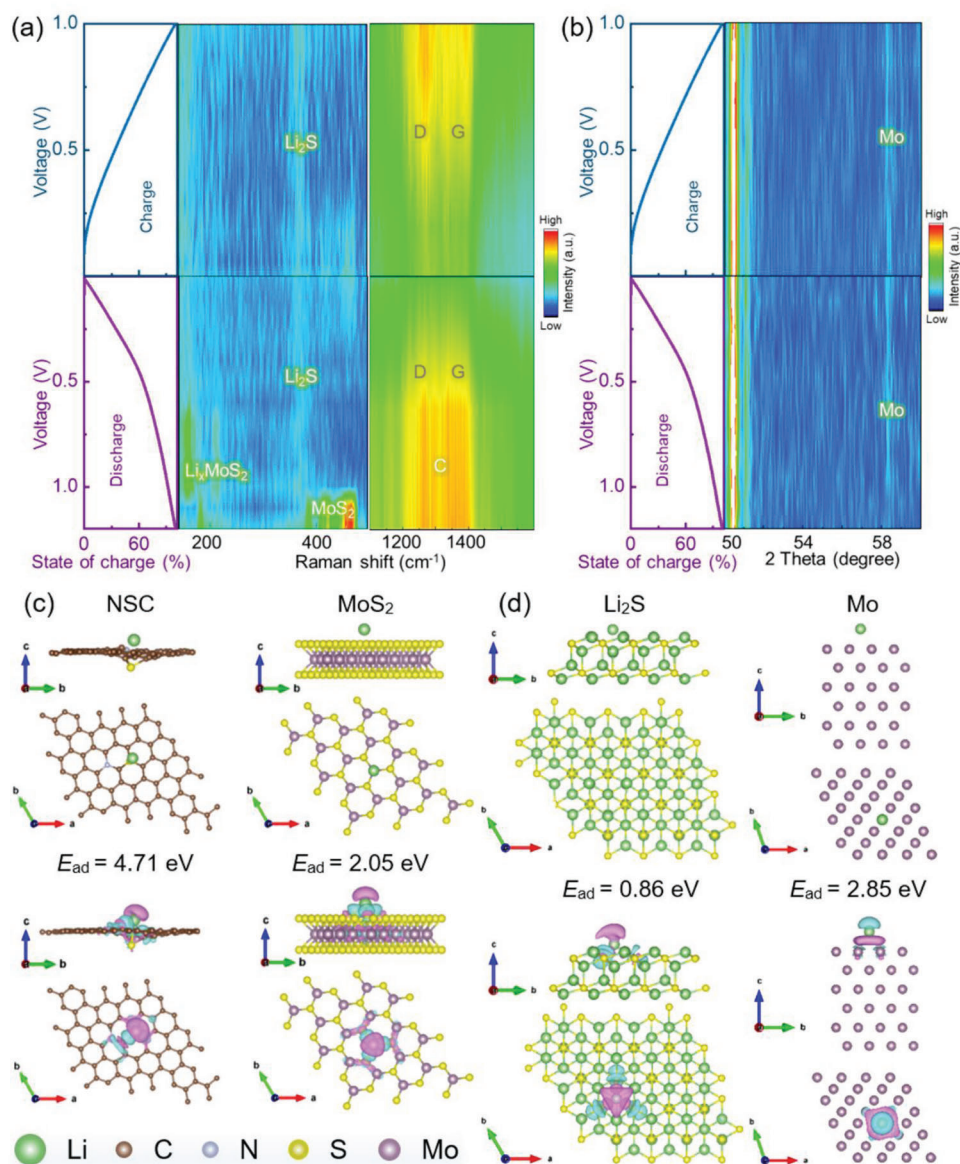


Figure 3. a) Galvanostatic charge–discharge (GCD) plots of the MoS₂@NSPCB host at 0.1 A g⁻¹ and the corresponding in situ Raman spectra. b) GCD plots of the MoS₂@NSPCB host at 0.1 A g⁻¹ and the corresponding in situ XRD patterns. Top and side views of different geometries, real-space charge densities, and E_{ad} values of Li atoms on c) NSC, MoS₂, d) Li₂S, Mo. The purple and blue colors, respectively, represent decreases and increases in the charge densities.

Supporting Information). A short-circuit eventually occurred after ≈65 h, causing a sudden drop in the voltage hysteresis.

The MoS₂@NSPCB host also endows the Li|Li cell with an excellent rate performance (Figure 2d), with stable working even at 30 mA cm⁻² with a low voltage overpotential below 100 mV. Electrochemical impedance spectroscopy (EIS) was employed to investigate the kinetics of charge transfer and Li-ion diffusion (Figure S10, Supporting Information). The Li|MoS₂@NSPCB cell shows a much smaller charge-transfer resistance (5.5 Ω) than the Li|MoO_x@NCF cell (27.2 Ω) at 30 °C, demonstrating the enhanced charge transport at the electrode/electrolyte interface. The activation energies for Li-ion diffusion within the different hosts were calculated based on the Arrhenius plots (Figure 2e).^[26]

The Li|MoS₂@NSPCB cell has a much smaller activation energy of 10.89 kJ mol⁻¹ than the Li|MoO_x@NCF cell (40.80 kJ mol⁻¹), suggesting that the continuous structure of the hierarchical porous nanobelts in the MoS₂@NSPCB host allows faster Li-ion diffusion. By virtue of the high porosity and controllable thickness, the MoS₂@NSPCB host enables the Li|Li symmetric cells to show good performance, even at a plating/stripping capacity of 3 mAh cm⁻² (Figure 2f). Long-term stabilities of over 1500 and 500 h were obtained at 3 and 10 mA cm⁻², respectively. The half-cell performance of the Li|Li symmetric cells using the MoS₂@NSPCB host is superior to similar cells using other hosts reported in the recent literature (Figure 2g; and Table S2, Supporting Information).^[27–35]

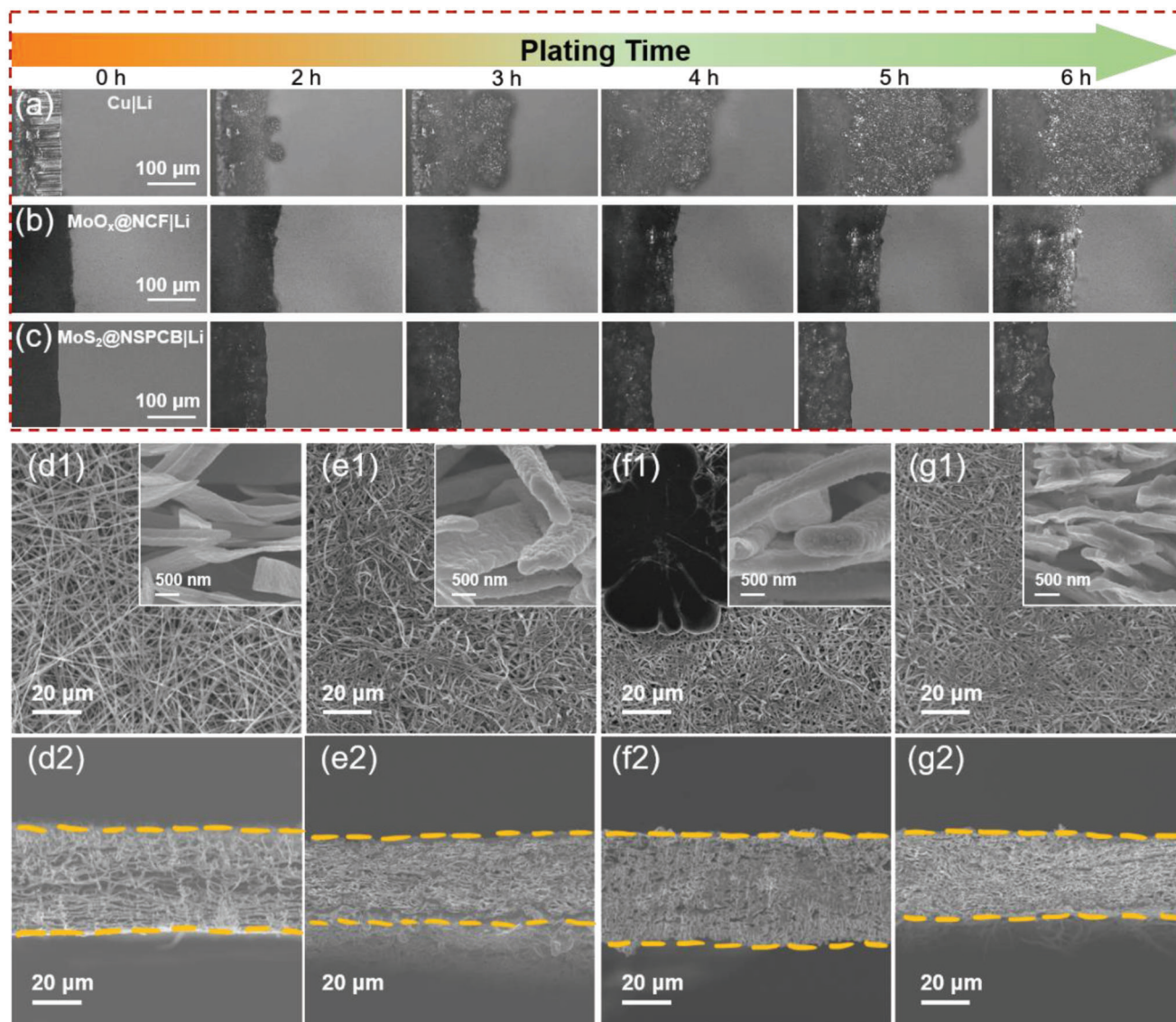


Figure 4. In situ optical microscopy of Li plating behavior on a) Cu foil, b) $\text{MoO}_x\text{@NCF}$, and c) $\text{MoS}_2\text{@NSPCB}$ at 1 mA cm^{-2} for 6 h. Ex situ surface and cross-section SEM images of the $\text{MoS}_2\text{@NSPCB}$ hosts: (d1, d2) before Li plating, (e1, e2) after Li plating with a capacity of 3 mAh cm^{-2} at 1 mA cm^{-2} , (f1, f2) after Li plating with a capacity of 6 mAh cm^{-2} at 1 mA cm^{-2} , and (g1, g2) after Li stripping with a capacity of 6 mAh cm^{-2} at 1 mA cm^{-2} .

Full cells were assembled using LiFePO_4 (LFP) as the cathode in order to evaluate the practical performance of the $\text{MoS}_2\text{@NSPCB}$ host-modified LMA ($\text{MoS}_2\text{@NSPCB-Li}$). The N/P ratio and electrolyte amount were fixed at 1:1 and $\approx 3.7\text{ }\mu\text{L mg}^{-1}$, respectively. The galvanostatic charge–discharge (GCD) profiles (Figure S11, Supporting Information) indicate that $\text{MoS}_2\text{@NSPCB-Li||LFP}$ exhibits a smaller voltage polarization than Cu-Li||LFP ($\approx 63.0\text{ mV}$ vs $\approx 90.0\text{ mV}$ at 1 C), highlighting the faster kinetics of the $\text{MoS}_2\text{@NSPCB}$ host. A high reversible capacity of $\approx 80\text{ mAh g}^{-1}$ is maintained even at 10 C , showing good rate capability. The $\text{MoS}_2\text{@NSPCB-Li||LFP}$ full cell can deliver a high energy of $\approx 460\text{ Wh kg}^{-1}$ based on the total weight of LFP and $\text{MoS}_2\text{@NSPCB-Li}$. Even after considering the weight of the current collectors, the $\text{MoS}_2\text{@NSPCB-Li||LFP}$ full cell can deliver an energy density of 348 Wh kg^{-1} , much higher than that of the

Cu-Li||LFP full cell (246 Wh kg^{-1}). The $\text{MoS}_2\text{@NSPCB-Li||LFP}$ pouch cell can easily power 68 LEDs and showed good bending performance by virtue of the self-standing properties of the $\text{MoS}_2\text{@NSPCB}$ host (Figure 2h). Moreover, the $\text{MoS}_2\text{@NSPCB-Li||LFP}$ full cell shows a remarkable cycling performance with a capacity retention of $\approx 70\%$ even after 1600 cycles at 10 C (Figure 2i).

The mechanism responsible for the modification of the $\text{MoS}_2\text{@NSPCB}$ host in LMAs was investigated using in situ Raman and XRD measurements on half cells. As shown in Figure 3a,b, MoS_2 is gradually lithiated, initially giving Li_xMoS_2 , which is finally transformed into Li_2S and Mo during the discharge process ($\text{MoS}_2 + 4\text{Li}^+ + 4\text{e}^- \rightarrow \text{Mo} + 2\text{Li}_2\text{S}$). The characteristic peaks of Li_2S and Mo are observed at low potential during the discharge process and the subsequent charge process, confirm-

ing their good stability as the active sites for regulating Li plating/stripping (Figure S14, Supporting Information). In addition, the high degree of recovery of the D and G bands in the Raman spectra suggests good reversibility of the change in the N,S-doped carbon framework. TEM images and the corresponding selected area electron diffraction results of the cycled MoS₂@NSPCB host further verify that the MoS₂ derivatives are uniformly anchored on the nanobelts with good structural integrity.

DFT calculations were used to probe the lithiophilicity and stability of the active sites within the MoS₂@NSPCB host. Models of Li atoms adsorbed on N,S-doped carbon (NSC), MoS₂, Li₂S, and Mo were constructed, and the optimized results are displayed in Figure 3c,d. The calculated adsorption energies (E_{ad}) of NSC and MoS₂ are 4.71 and 2.05 eV, respectively, indicating that the N/S heteroatoms and MoS₂ are good lithiophilic sites that can adsorb Li ions on the interface between the electrode and electrolyte in the initial cycle. As compared with N/S heteroatoms, Li₂S and Mo show a lower E_{ad} of 0.86 and 2.85 eV, respectively. The moderate Li adsorption of these materials is beneficial to both Li plating and stripping because of the low nucleation/diffusion barriers of Li and good chemical stability to Li.^[36] Although the N,S doping is not favorable for Li diffusion and striping, it enables good carbon support which firmly anchors the ideal lithiophilic sites (MoS₂ derivatives). The structural stability of the lithiophilic sites was further revealed by comparing the E_{ad} of active sites on a pure carbon support (C) and NSC (Figure S15, Supporting Information). The N,S-doped carbon has a higher E_{ad} than the undoped carbon, confirming that the lithiophilic sites in the MoS₂@NSPCB host have both high surface activity and good structural stability, thus efficiently guiding uniform Li nucleation and facilitating highly reversible Li plating/stripping.^[37]

In situ optical microscopy was further performed to investigate the inhibitory effects of the hosts on Li dendrites. As shown in Figure 4a, Li dendrites formed quickly on the Cu surface, resulting in a highly porous structure with a large volume change. Although Li dendrites were not observed on the MoO_x@NCF host in the initial plating process, obvious volumetric expansion and surface Li dendrite formation were eventually observed due to the limited space for Li growth (Figure 4b). In contrast, a smooth surface without any observable dendrites was observed for the MoS₂@NSPCB host throughout the entire deposition process (Figure 4c). This shows that the self-standing MoS₂@NSPCB host with its abundant lithiophilic sites and 3D porous structure favors homogeneous Li plating and suppresses the formation of Li dendrites.

Ex situ SEM images for different Li plating/stripping states clearly show the morphological evolution of the MoS₂@NSPCB host. As shown in Figure 4d, the host has an initial thickness of ≈ 40 μm with an ultrathin nanobelt structure; After a deposition capacity of 3 mAh cm⁻², the host thickness of MoS₂@NSPCB decreases due to the pressure within the cells, while the compactness of the host increases significantly (Figure 4e2). In addition, the thickness of the nanobelt increases from ≈ 100 to ≈ 300 nm, showing the uniform Li plating (Figure 4e1, inset). At a higher deposition capacity of 6 mAh cm⁻², the host thickness increases slightly, and some Li deposits with an island-like structure are observed on the host surface (Figure 4f). The nanobelt still exhibits a smooth surface with a thickness of 500–600 nm (Figure 4f, inset). After Li stripping with a capacity of 6 mAh cm⁻², the thick-

ness of the host and nanobelt decreases to ≈ 30 and ≈ 100 nm, respectively (Figure 4g). The good structural stability and high Li-plating/stripping reversibility of the MoS₂@NSPCB host endow the LMAs with excellent cycling performance.

3. Conclusions

We have fabricated a self-standing MoS₂@NSPCB host for LMAs using an efficient sulfate-assisted method. LMAs using the MoS₂@NSPCB host remain dendrite-free with good half-cell and full-cell performance. A detailed physicochemical study has shown that the N,S-doped carbon nanobelts firmly anchor the MoS₂-derived lithiophilic sites, which homogenize the Li nucleation and suppress the formation of Li dendrites. In addition, the presence of a conductive 3D structure with hierarchical porosity accelerates Li-ion diffusion and accommodates the volume changes of the Li deposits. This work has not only proposed a new self-standing host for LMAs but also suggested new ideas for the modification of other metallic anodes.

4. Experimental Section

Synthesis of MoS₂@NSPCB: An aqueous gelatin solution (15 wt%, 9 mL) was mixed with Na₂SO₄ (570 mg) and (NH₄)₆Mo₇O₂₄·4H₂O (700 mg) by stirring at 60 °C for 1 h. The solution was used to electrospin films (ET2535X, Ucalery). The gelatin films obtained after electrospinning for 6 h were stabilized by heating at 270 °C for 1 h in air, followed by pyrolysis at 700 °C for 1 h under an argon atmosphere (heating rate: 2.5 °C min⁻¹). The pyrolyzed samples were washed by water and dried overnight at 60 °C.

Synthesis of NSPCB and MoO_x@NCF: The preparation procedures were similar to that for MoS₂@NSPCB. NSPCB and MoO_x@NCF were prepared without adding (NH₄)₆Mo₇O₂₄·4H₂O and Na₂SO₄, respectively.

Supporting Information

Supporting Information is available from the Wiley Online Library or from the author.

Acknowledgements

B.L. and W.C. contributed equally to this work. This work was supported by National Natural Science Foundation of China (Nos. 52130206, U20A20337, 22178016, 52003025, and 52002012), the Fundamental Research Funds for the Central Universities (No. buctrc202024, JD2211), and the high-performance computing platform of BUCT.

Conflict of Interest

The authors declare no conflict of interest.

Data Availability Statement

The data that support the findings of this study are available from the corresponding author upon reasonable request.

Keywords

carbon nanobelts, heteroatom doping, Li metal anode, lithiophilic site, self-standing host

Received: July 24, 2022

Revised: August 24, 2022

Published online: September 25, 2022

- [1] C. Fu, S. Lin, C. Zhao, J. Wang, L. Wang, J. L. Bao, Y. Wang, T. Liu, *Energy Storage Mater.* **2022**, *45*, 1109.
- [2] C. Wang, M. Liu, M. Thijs, F. G. B. Ooms, S. Ganapathy, M. Wage-maker, *Nat. Commun.* **2021**, *12*, 6536.
- [3] G. M. Hobold, J. Lopez, R. Guo, N. Minafra, A. Banerjee, Y. M. Shirley, Y. Shao-Horn, B. M. Gallant, *Nat. Energy* **2021**, *6*, 951.
- [4] J. Cao, Y. Xie, Y. Yang, X. Wang, W. Li, Q. Zhang, S. Ma, S. Cheng, B. Lu, *Adv. Sci.* **2022**, *9*, 2104689.
- [5] Q. P. Wu, Y. J. Zheng, X. Guan, J. Xu, F. H. Cao, C. L. Li, *Adv. Funct. Mater.* **2021**, *31*, 2101034.
- [6] Q. F. Yang, M. N. Cui, J. L. Hu, F. L. Chu, Y. J. Zheng, J. J. Liu, C. L. Li, *ACS Nano* **2020**, *14*, 1866.
- [7] J. W. Meng, C. L. Li, *Energy Storage Mater.* **2021**, *37*, 466.
- [8] Z. Guo, Y. Pang, S. Xia, F. Xu, J. Yang, L. Sun, S. Zheng, *Adv. Sci.* **2021**, *8*, 2100899.
- [9] S. Kim, J. S. Kim, L. Miara, Y. Wang, S. K. Jung, S. Y. Park, Z. Song, H. Kim, M. Badding, J. Chang, V. Roev, G. Yoon, R. Kim, J. H. Kim, K. Yoon, D. Im, K. Kang, *Nat. Commun.* **2022**, *13*, 1883.
- [10] M. Huang, Z. Yao, Q. Yang, C. Li, *Angew. Chem., Int. Ed.* **2021**, *60*, 14040.
- [11] S. Auffarth, W. Daffinger, J. Mehler, V. Ardizzon, P. Preuster, P. Wasserscheid, S. Thiele, J. Kerres, *J. Mater. Chem. A* **2022**, *10*, 17208.
- [12] Y. Fang, S. L. Zhang, Z. P. Wu, D. Luan, X. W. Lou, *Sci. Adv.* **2021**, *7*, eabg3626.
- [13] H. Lin, Z. Zhang, Y. Wang, X. L. Zhang, Z. Tie, Z. Jin, *Adv. Funct. Mater.* **2021**, *31*, 2102735.
- [14] Y. Mei, J. Zhou, Y. Hao, X. Hu, J. Lin, Y. Huang, L. Li, C. Feng, F. Wu, R. Chen, *Adv. Funct. Mater.* **2021**, *31*, 2106676.
- [15] C. Chen, J. Guan, N. W. Li, Y. Lu, D. Luan, C. H. Zhang, G. Cheng, L. Yu, X. W. Lou, *Adv. Mater.* **2021**, *33*, 2100608.
- [16] H. Kwon, J. H. Lee, Y. Roh, J. Baek, D. J. Shin, J. K. Yoon, H. J. Ha, J. Y. Kim, H. T. Kim, *Nat. Commun.* **2021**, *12*, 5537.
- [17] T. S. Wang, X. Liu, Y. Wang, L. Z. Fan, *Adv. Funct. Mater.* **2021**, *31*, 2001973.
- [18] Y. Deng, J. Gao, M. Wang, C. Luo, C. Zhou, M. Wu, *Energy Storage Mater.* **2022**, *48*, 114.
- [19] T. Zhou, J. Shen, Z. Wang, J. Liu, R. Hu, L. Ouyang, Y. Feng, H. Liu, Y. Yu, M. Zhu, *Adv. Funct. Mater.* **2020**, *30*, 1909159.
- [20] K. Li, Z. Hu, J. Ma, S. Chen, D. Mu, J. Zhang, *Adv. Mater.* **2019**, *31*, 1902399.
- [21] Y. Liu, S. Wang, X. Sun, J. Zhang, F. uz Zaman, L. Hou, C. Yuan, *Energy Environ. Mater.* **2022**, <https://doi.org/10.1002/eem2.12263>
- [22] B. Zhang, L. Qin, Y. Fang, Y. Chai, X. Xie, B. Lu, S. Liang, J. Zhou, *Sci. Bull.* **2022**, *67*, 955.
- [23] S. M. Lee, J. Kim, J. Moon, K. N. Jung, J. H. Kim, G. J. Park, J. H. Choi, D. Y. Rhee, J. S. Kim, J. W. Lee, M. S. Park, *Nat. Commun.* **2021**, *12*, 39.
- [24] D. C. Nguyen, T. L. Luyen Doan, S. Prabhakaran, D. T. Tran, D. H. Kim, J. H. Lee, N. H. Kim, *Nano Energy* **2021**, *82*, 105750.
- [25] A. Shan, X. Teng, Y. Zhang, P. Zhang, Y. Xu, C. Liu, H. Li, H. Ye, R. Wang, *Nano Energy* **2022**, *94*, 106913.
- [26] R. Wang, J. Yu, J. Tang, R. Meng, L. F. Nazar, L. Huang, X. Liang, *Energy Storage Mater.* **2020**, *32*, 178.
- [27] Y. Qian, Z. Zhu, Y. Li, Z. Pan, L. Wang, J. Tian, H. Zhou, N. Lin, Y. Qian, *Energy Storage Mater.* **2022**, *47*, 620.
- [28] J. Wu, Z. Rao, X. Liu, Y. Shen, C. Fang, L. Yuan, Z. Li, W. Zhang, X. Xie, Y. Huang, *Adv. Mater.* **2021**, *33*, 2007428.
- [29] J. Qian, S. Wang, Y. Li, M. Zhang, F. Wang, Y. Zhao, Q. Sun, L. Li, F. Wu, R. Chen, *Adv. Funct. Mater.* **2021**, *31*, 2006950.
- [30] C. Wei, H. Fei, Y. Tian, Y. An, H. Guo, J. Feng, Y. Qian, *Energy Storage Mater.* **2020**, *26*, 223.
- [31] P. Gao, H. Wu, X. Zhang, H. Jia, J. M. Kim, M. H. Engelhard, C. Niu, Z. Xu, J. G. Zhang, W. Xu, *Angew. Chem., Int. Ed.* **2021**, *60*, 16506.
- [32] Y. Fang, Y. Zeng, Q. Jin, X. F. Lu, D. Luan, X. Zhang, X. W. Lou, *Angew. Chem., Int. Ed.* **2021**, *60*, 8515.
- [33] X. He, S. Jin, L. Miao, Y. Cai, Y. Hou, H. Li, K. Zhang, Z. Yan, J. Chen, *Angew. Chem., Int. Ed.* **2020**, *59*, 16705.
- [34] T. Yang, L. Li, T. Zhao, Y. Ye, Z. Ye, S. Xu, F. Wu, R. Chen, *Adv. Energy Mater.* **2021**, *11*, 2102454.
- [35] Z. Huang, Z. Li, M. Zhu, G. Wang, F. Yu, M. Wu, G. Xu, S. X. Dou, H. K. Liu, C. Wu, *Nano Lett.* **2021**, *21*, 10453.
- [36] L. Yu, Q. Su, B. Li, L. Huang, G. Du, S. Ding, W. Zhao, M. Zhang, B. Xu, *Chem. Eng. J.* **2022**, *429*, 132479.
- [37] S. Q. Li, L. Zhang, T. T. Liu, Y. W. Zhang, C. Guo, Y. Wang, F. H. Du, *Adv. Mater.* **2022**, *34*, 2201801.